Phonon induced rank-2 U(1) nematic liquid states

Han Yan (闫寒)[1,2,*] and Andriy H. Nevidomskyy[2]
[1]*Rice Academy of Fellows, Rice University, Houston, Texas 77005, USA*
[2]*Department of Physics & Astronomy, Rice University, Houston, Texas 77005, USA*

(Received 4 December 2022; revised 4 May 2023; accepted 3 January 2024; published 1 February 2024)

Fascinating new phases of matter can emerge from strong electron interactions in solids. In recent years, a new exotic class of many-body phases, described by generalized electromagnetism of symmetric rank-2 electric and magnetic fields and immobile charge excitations dubbed *fractons*, has attracted wide attention. Besides having interesting properties in their own right, the models with generalized electromagnetism are also closely related to gapped fracton quantum orders, new phases of dipole-covering systems, as well as quantum information and quantum gravity. However, experimental realization of the rank-2 U(1) gauge theory is still absent and even known practical experimental routes are scarce. In this work, we propose a scheme of coupled optical phonons and nematic degrees of freedom, as well as several concrete experimental platforms for their realizations. We show that these systems can realize the electrostatics sector of the rank-2 U(1) gauge theory. A great advantage of the proposed scheme is that it requires only the basic ingredients of phonon and nematic physics, and hence may be applicable to a wide range of experimental realizations from liquid crystals to electron orbitals.

DOI: 10.1103/PhysRevB.109.075102

I. INTRODUCTION

At the forefront of modern physics lies the concept of emergence—the spontaneous appearance of qualitative changes in the behavior of large, complex systems that can by no means be inferred by extrapolating the properties of only a few particles [1]. The emergent behavior is codified by the new "laws" in an effective theory, and the emergent phases often transcend the traditional Landau-Ginzburg paradigm of symmetry breaking. One example of such an emergent phase is the spin liquids—exotic states built on quantum superposition of product states, characterized not by any order parameter, but by the topological entanglement and topological order. A subclass of such spin liquids can be described by local constraints on the local degrees of freedom (DoF), leading to the emergence of a gauge-invariant description, and thereby to topological orders, fractionalized excitations, and long-range entanglement [2–5]. A well-known example is quantum spin ice on the pyrochlore lattice, which realizes U(1) Maxwell gauge theory [6]. It hosts emergent excitations mimicking the Maxwell electrodynamics: photons, electric charges, and even magnetic monopoles. As such, it has been under intense theoretical [3–15] and experimental [16–24] investigation.

Recently, a class of more exotic forms of emergent electrodynamics proposed as effective theories for spin liquid phases [25–28] has attracted considerable attention. As a generalization of Maxwell electrodynamics, it features electric and gauge fields in the form of rank-2 (R2) or, generally, higher-rank symmetry tensors. The correspondingly modified Gauss's conservation laws result in some unexpected, exciting properties. The electric charge excitations dubbed *fractons* are intrinsically constrained from moving in the system and foreshadow a new class of gapped fracton quantum liquid order beyond topological order [29–40]. The rank-2 U(1) (R2-U1) theories are also shown to be akin to gravity [25,41–43], and related to new phases of matter featuring dipole conserving dynamics [44–48].

However, these remarkable properties come with a cost: the central ingredient—local constraints applied to tensors—is in a more complex form than the traditional Gauss's law of Maxwell electromagnetism. To enforce these constraints, complicated multibody interactions are required in many prototypical fracton models [25,27,29,31–33,49,50], while experimental proposals remain scarce [37,38,51]. Therefore, concrete designs for experimental realizations of R2-U1 phases pose a significant challenge, and overcoming this difficulty would constitute a crucial step for future development of the field.

Here we propose a realistic experimental scheme to achieve nematic liquid states described by the classical limit R2-U1 theory, which is realizing the electrostatics of such higher-rank theories. Phases of matter with nematic DoF, such as liquid crystals, are good potential candidates for this purpose since they are naturally represented by symmetric tensors—exactly those needed in the R2-U1 physics. The challenge is to find a realistic approach toward the specific low-energy Hamiltonian that would give rise to a nematic liquid state obeying the R2-U1 Gauss's law, instead of driving the system into an ordered state.

In this work, we show that this is readily achievable. The ingredients in our model are quite common: Einstein phonons and the most general coupling between phonons and nematic DoFs. We demonstrate that integrating out the phonon modes leads precisely to the sought Gauss's law-enforcing term on

*hy41@rice.edu

the remaining nematic DoFs. In addition to the idealized effective theory, we present a few concrete experimental platforms where such a theory can be realized. Our approach has the advantage of having a wide range of applicability. The existence of nematics at different scales—from electron orbitals to organic molecules to soft matter—means that our proposed design can be realized in a variety of experimental platforms. Different types of available nematic matters also enable us to construct different versions of R2-U1 theories. We hope that our work opens a gateway to experimental realizations of generalized higher-rank gauge theories.

II. THE IDEALIZED MODEL

A. Hamiltonian of nematic-phonon coupling

The idealized model Hamiltonian to realize the R2-U1 physics via nematic-phonon coupling is composed of three parts: optical phonons, the nematic degrees of freedom, and their coupling:

$$\begin{aligned}\mathcal{H} &= \mathcal{H}_{\text{ph}} + \mathcal{H}_{\text{ph-nem}} + \mathcal{H}_{\text{nem}} \\ &= \frac{\boldsymbol{\Pi}^2}{2m_{\text{ph}}} + \frac{m_{\text{ph}}\omega_0^2}{2}\boldsymbol{u}\cdot\boldsymbol{u} - \lambda\varepsilon_{ij}\Phi_{ij} + M\sum_{i\leqslant j}\Phi_{ij}^2, \end{aligned} \tag{1}$$

where m_{ph} is the atomic mass density corresponding to the phonon mode, $\boldsymbol{u}(\boldsymbol{r})$ is the lattice distortion of the Einstein phonons (i.e., phonons with a flat energy dispersion $\hbar\omega_0$), and $\boldsymbol{\Pi}$ is the canonically conjugate momentum. We have suppressed the phonon polarization index and assumed a single optical branch for simplicity. The second term $\mathcal{H}_{\text{ph-nem}}$ is the leading-order coupling between the nematic DoF described by the symmetric tensor Φ_{ij} [52–56] and the strain tensor of the lattice distortion,

$$\varepsilon_{ij}(\boldsymbol{r}) = \partial_i u_j(\boldsymbol{r}) + \partial_j u_i(\boldsymbol{r}). \tag{2}$$

The third term $\mathcal{H}_{\text{nem}}$ has the meaning of a mass term for the nematic degrees of freedom and is assumed to be positive definite ($M > 0$). This term can also be thought of as imposing a physical constraint on the tensor to be of finite length, which occurs naturally in certain types of nematic matter (see Sec. VI for details). In this work, we explicitly assume no spontaneous breaking of the rotational symmetry, i.e., we always assume nematic fluctuations without the long-range nematic order [57].

In what follows, we suppress the dynamical terms associated with the phonon and nematic degrees of freedom (written here in the Lagrangian form),

$$\mathcal{L}_{\text{dynamics}} = \frac{m_{\text{ph}}}{2}(\partial_t \boldsymbol{u})^2 + \frac{m}{2}(\partial_t \boldsymbol{\Phi})^2, \tag{3}$$

since we are chiefly interested in the classical sector of the system. Above, m is the kinetic mass of the nematic degrees of freedom. The role of these terms in the dynamics in a quantum system is discussed in more detail in Sec. VI.

The spectrum of the diagonalized Hamiltonian in a square lattice is shown in Figs. 1(f) and 1(g) (see Fig. 3 for the square lattice setup). The false color indicates the distribution on each band of the correlator $\langle\Phi_{xx}(-\boldsymbol{q})\Phi_{yy}(\boldsymbol{q})\rangle$, whose meaning will be clarified in a later part of this section.

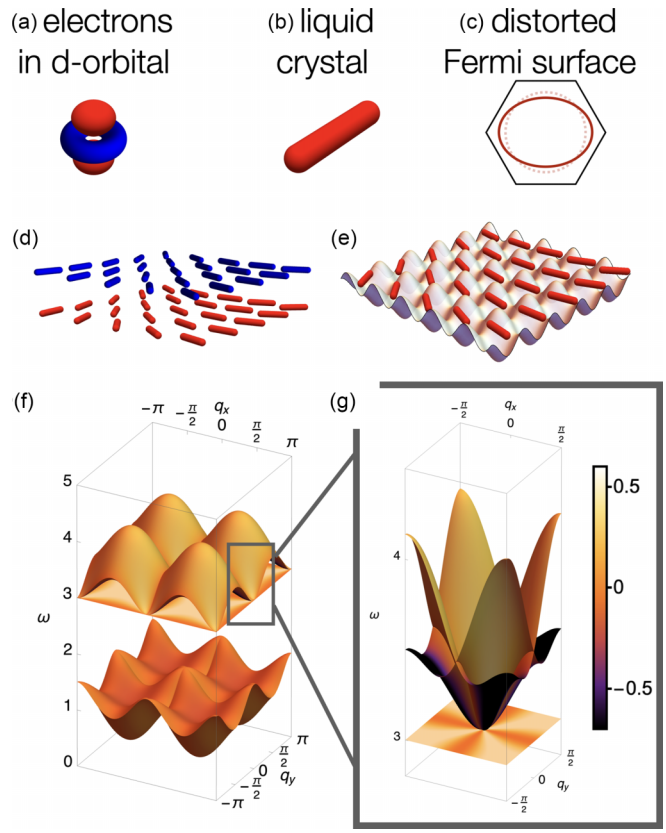

FIG. 1. Realizing rank-2 U(1) electrostatics via optical phonon-nematic coupling. (a)–(c) Examples of microscopic objects with nematic degrees of freedom. (d) Bilayer nematic as a representative experimental construction that realizes the ideal model [Eq. (1)]. (e) Nematic layer trapped in an artificial periodic potential as a representative experimental construction. (f) The band structure of Eq. (1). (g) Zoomed-in view of the phonon-nematic band structure, in which the flat band corresponds to the vector-charge-free nematic configurations, and the upward dispersing bands correspond to the charged nematic configurations.

By integrating out the Gaussian phonon modes, we end up with the effective theory for the nematic DoF only, described by the Hamiltonian

$$\mathcal{H}_{\text{nem-eff}} = \Lambda(\partial_i\Phi_{ij})(\partial_k\Phi_{kj}) + M\sum_{i\leqslant j}\Phi_{ij}^2, \tag{4}$$

where $\Lambda = \lambda^2/(2m_{\text{ph}}\omega_0^2)$. In the limit of sufficiently large $\Lambda \gg T$ relative to the temperature, the first term imposes a high energy cost for Φ_{ij} configurations that violate the constraint

$$\partial_i\Phi_{ij} = 0. \tag{5}$$

Upon identifying the nematic DoF with the generalized rank-2 electric field $\Phi_{ij} \longleftrightarrow E_{ij}$, its derivative becomes associated with the generalized vector charge,

$$\partial_i\Phi_{ij} \longleftrightarrow \rho_j \equiv \partial_i E_{ij}, \tag{6}$$

and Eq. (5) becomes exactly the Gauss's law for the vector-charged R2-U1 theory. Hence, the classical R2-U1 nematic liquid state is realized in the low-energy sector of the theory.

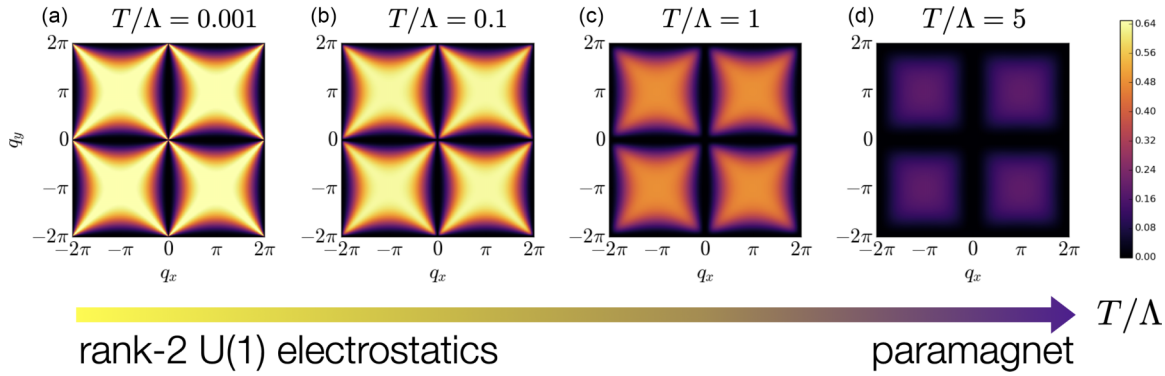

FIG. 2. Nematic correlation functions $\langle \Phi_{xx}(-\boldsymbol{q})\Phi_{yy}(\boldsymbol{q})\rangle$ for the model in Eq. (4). The four panels show the correlation functions, using a false-color map, computed via the self-consistent Gaussian approximation (see Appendix B) on a square lattice (Fig. 3) at different temperatures relative to the parameter Λ. The high-temperature regime shown in (d) is a paramagnetic phase with vanishing correlations. The low-temperature regime shown in (a) is the rank-2 U(1) phase, manifested by the characteristic fourfold pinch point pattern in the correlation function around $\boldsymbol{q} = \boldsymbol{0}$, originating from the functional form $\langle \Phi_{xx}(-\boldsymbol{q})\Phi_{yy}(\boldsymbol{q})\rangle \propto q_x^2 q_y^2/q^4$. (b), (c) The fourfold pinch points become gradually smeared due to thermal fluctuations at intermediate temperatures.

A more physical interpretation of the model is achieved by noticing that

$$-\lambda \varepsilon_{ij}\Phi_{ij} = 2\lambda \boldsymbol{u}\cdot\boldsymbol{\rho} + \text{total derivative}. \tag{7}$$

This means the vector-charge excitation $\boldsymbol{\rho}$ is linearly coupled to the lattice distortion. The energy cost of the lattice distortion induces, upon integrating out the lattice DoF, the potential energy $\lambda^2\boldsymbol{\rho}^2/(2\rho\omega_0^2)$ for the charge excitations.

B. Experimental signatures

To quantitatively show the emergence of R2-U1 electrostatics, we study the model of Eq. (4) on a square lattice under the on-site constraint $\sum_{i\leqslant j}\Phi_{ij}(\boldsymbol{r})^2 = 1$ and examine its correlation function $\langle \Phi_{ij}(-\boldsymbol{q})\Phi_{kl}(\boldsymbol{q})\rangle$ at different temperatures using the self-consistent Gaussian approximation (SCGA, described in Appendix B). Depending on the microscopic origin of the nematics, there are different ways to measure the correlation functions in an experiment. For example, in liquid crystals, one can use polarized light to obtain the so-called Schlieren texture [58,59], which can be used to reconstruct the real-space configuration of the nematics.

The equal time correlation function $\langle \Phi_{ij}(-\boldsymbol{q})\Phi_{kl}(\boldsymbol{q})\rangle$ in the R2-U1 phase is constrained by the Gauss's law $q_\alpha\langle \Phi_{ij}(-\boldsymbol{q})\Phi_{kl}(\boldsymbol{q})\rangle = 0$, where α is one of the four indices i, j, k, l and the repeated index is summed over. As a consequence, the correlation is restricted to be proportional to a highly anisotropic projector in the form of

$$\begin{aligned}&\langle \Phi_{ij}(-\boldsymbol{q})\Phi_{kl}(\boldsymbol{q})\rangle \\ &\quad\propto \frac{1}{2}(\delta_{ik}\delta_{jl}+\delta_{il}\delta_{jk}) + \frac{q_iq_jq_kq_l}{q^4} \\ &\quad\quad -\frac{1}{2}\left(\delta_{ik}\frac{q_jq_l}{q^2}+\delta_{jk}\frac{q_iq_l}{q^2}+\delta_{il}\frac{q_jq_k}{q^2}+\delta_{jl}\frac{q_iq_k}{q^2}\right).\end{aligned} \tag{8}$$

In particular, $\langle \Phi_{xx}(-\boldsymbol{q})\Phi_{yy}(\boldsymbol{q})\rangle \propto q_x^2q_y^2/q^4$ shows a characteristic pattern dubbed "fourfold pinch point" [60–62].

In Fig. 2, we present the correlation function $\langle \Phi_{xx}(-\boldsymbol{q})\Phi_{yy}(\boldsymbol{q})\rangle$, computed within the SCGA approach, at different ratios of T/Λ. As the result demonstrates, at high temperature, the system is a paramagnet and the correlation function is essentially vanishing. At low temperatures, on the other hand, the fourfold pinch point emerges as the system enters the R2-U1 phase. The transition between the two phases is expected to be not a phase transition, but a crossover.

The same fourfold pinch point is also visible in the band structure of the diagonalized Hamiltonian, shown in Figs. 1(f) and 1(g). There, the flat band corresponds to the nematic states obeying Gauss's law. Note that the energy of this flat band is finite due to the nonzero mass M in Eq. (4), and the lack of dispersion is due to the fact that the mass term imposes a local constraint, i.e., all such states are momentum independent. The fourfold pinch point is imprinted on the flat band, which is consistent with the result from the Gaussian-integrated theory [Eq. (4)].

C. Effects of perturbations

The idealized model of Eq. (1) is fine tuned. For example, if there are symmetry-breaking terms, the nematic DoFs, instead of fluctuating subject to the Gauss's law, can become ordered at sufficiently low temperature [this would require setting mass $M < 0$ and adding quartic terms to the Hamiltonian in Eq. (1)]. Hence, we must address the question of whether the idealized model can be realized experimentally.

We remark that it should not be surprising that generally speaking, the Hamiltonian realizing such classical spin/nematic liquid requires fine tuning. A well-known canonical example is the classical spin ice [63], whose exact macroscopic ground-state degeneracy is the consequence of fine-tuned interactions and can be lifted by the addition of arbitrarily small terms to the Hamiltonian. The U(1) gauge theory being gapless, there is no protection against such terms in general. However, as long as these terms have a magnitude smaller than the experimentally accessible temperature, their effect is not strong enough to drive the system into, e.g., an ordered state, and the relevant degrees of freedom fluctuate, subject to the constraint imposed by the Gauss's law. This

general principle applies equally to the spin ice and to our model of generalized higher-rank U(1) theory.

D. Effects of discrete crystalline symmetry

The coupling between lattice and nematic DoFs will often lower the symmetry of the nematic order parameter from U(1) to a discrete one. If the energy scale of such symmetry breaking is significantly lower than the temperature of interest, it can be effectively neglected. However, in the opposite case, more care is needed to determine if the rank-2 U(1) Gauss's law description still holds. Systems with discretized nematic DoFs can still be in a rank-2 U(1) spin liquid phase, if the exponentially degenerate ground states still exist, and are described by the rank-2 U(1) Gauss's law. This is similar to spin ice and checkerboard ice spin liquids, which are Ising spin systems described by Maxwell's U(1) Gauss's law, $\partial_i E_i = 0$. The most essential requirement is that flipping a local patch of spins follows the pattern of the magnetic field $\boldsymbol{B} = \nabla \times \boldsymbol{A}$. In terms of the lattice spins, this is to flip spins connected head to tail on a closed loop. The similar principle applies to rank-2 U(1) spin liquids too. Here, let us give an example of such spin liquid arising from discretized nematic DoFs. We consider a square lattice, with nematic DoFs sitting on the vertices and plaquette centers of the lattice [Fig. 3(a)]. We then assume the vertex nematics can only take a finite range of integer values (for example, $-1, 0, 1$) for its Φ_{xx} and Φ_{yy} components, and the plaquette nematics for its Φ_{xy} components, as a consequence of the lattice symmetry. The phonon-intermediated interactions are $\rho_x^2 + \rho_y^2$, where

$$\begin{aligned} \rho_x &= \partial_x \Phi_{xx} + \partial_y \Phi_{yx}, \\ \rho_y &= \partial_y \Phi_{yy} + \partial_x \Phi_{xy}, \end{aligned} \tag{9}$$

and on lattice, their discretized version becomes

$$\begin{aligned} \rho_x(\boldsymbol{R}) &= \Phi_{xx}(\boldsymbol{R} + \hat{\boldsymbol{x}}/2) - \Phi_{xx}(\boldsymbol{R} - \hat{\boldsymbol{x}}/2) \\ &\quad + \Phi_{yx}(\boldsymbol{R} + \hat{\boldsymbol{y}}/2) - \Phi_{yx}(\boldsymbol{R} - \hat{\boldsymbol{y}}/2), \\ \rho_y(\boldsymbol{R}) &= \Phi_{yy}(\boldsymbol{R} + \hat{\boldsymbol{y}}/2) - \Phi_{yy}(\boldsymbol{R} - \hat{\boldsymbol{y}}/2) \\ &\quad + \Phi_{xy}[(\boldsymbol{R} + \hat{\boldsymbol{x}}/2)] - \Phi_{xy}[(\boldsymbol{R} - \hat{\boldsymbol{x}}/2)]. \end{aligned} \tag{10}$$

The definition of $\boldsymbol{\rho}$ is illustrated in Figs. 3(a) and 3(b). The ground states are nematic configurations where the condition $\rho_{x,y} = 0$ is satisfied at every site. Next, we examine the ground-state degeneracy structure. That is, we search for the minimal change of Φ_{ij} that takes one ground-state configuration to another. We found this operation, expressed in terms of operators $\Phi_{ij}^{\pm}$ that increase/decrease the value of Φ_{ij} by one, to be that shown in Fig. 3(e). This is exactly the magnetic field for the rank-2 U(1) theory,

$$B = \epsilon_{ab}\epsilon_{cd}\partial^a \partial^c A^{bd}, \tag{11}$$

where A^{bd} is the conjugate of E_{ij}. To see this more clearly, we notice that the two terms in B are

$$\epsilon_{cd}\partial^c A^{xd} = \partial_x A^{xy} - \partial_y A^{xx}, \tag{12}$$

$$\epsilon_{cd}\partial^c A^{yd} = \partial_x A^{yy} - \partial_y A^{yx}. \tag{13}$$

The first one corresponds to Fig. 3(c) and the second one corresponds to Fig. 3(d). Hence, $B = \epsilon_{ab}\epsilon_{cd}\partial^a \partial^c A^{bd}$ is curl as four of such operations tiled together shown in Fig. 3(e). We can then conclude that this model of discretized nematic DoFs is also in a rank-2 U(1) nematic liquid phase. More generally, whether the rank-2 U(1) nematic liquid phase survives after the continuous nematic DoFs breaks down to discrete ones depends on the specific details of the symmetry breaking.

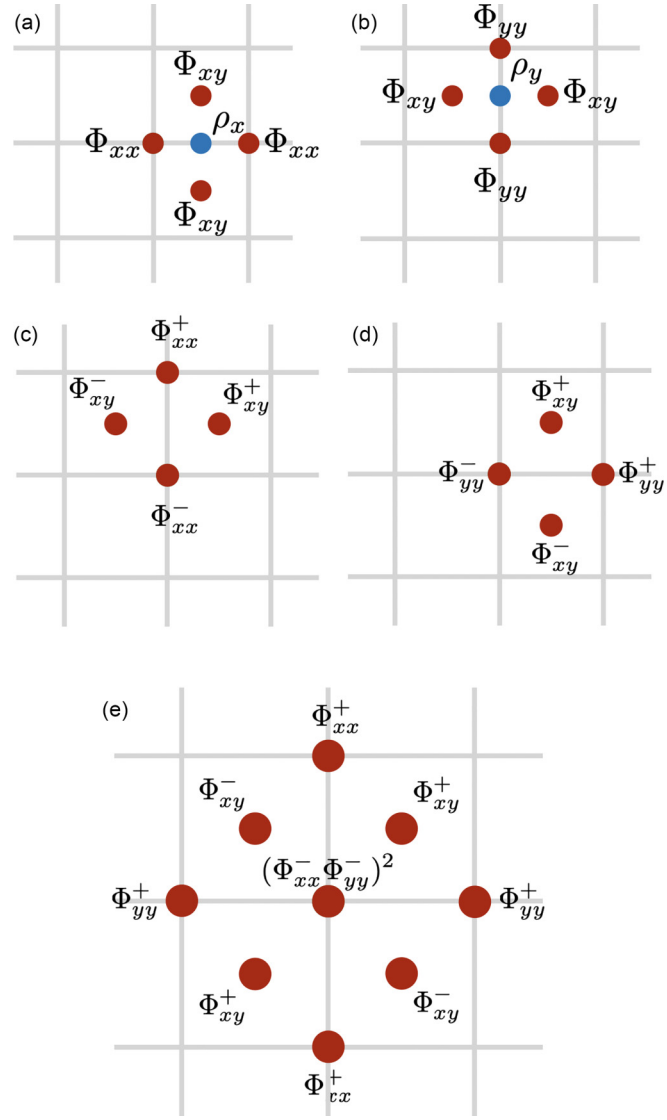

FIG. 3. The square lattice model with nematic degrees of freedom. (a), (b) Nematic degrees of freedom Φ_{xx} and Φ_{yy} defined on the vertices of the lattice, with off-diagonal components Φ_{xy} situated in the centers of the plaquettes. The lattice representation of the vector charge $\boldsymbol{\rho}$ in Eq. (6) has two components, $\boldsymbol{\rho} = (\rho_x, \rho_y)$, which live on the x and y links of the lattice, respectively, based on the four Φ_{ij} surrounding it. This model is used for computing the correlation functions in Eq. (8) and throughout the paper. (c), (d) Spin flipping terms correspond to Eqs. (12), (13) for discretized Φ_{ij}. These terms are the products of four $\phi_{ij}^{\pm}$ operators each. (e) Spin flipping term that acts as the gauge-invariant magnetic field in the generalized rank-2 electrodynamics [Eq. (11)]. This term is a product of 12 $\phi_{ij}^{\pm}$ operators shown. When acting on a Gauss's law-obeying charge-free electric field configuration, the state is mapped onto another charge-free configuration.

Following the above example, one can design rank-2 U(1) nematic liquid phases for discrete nematic DoFs too.

III. ADVANTAGES AND CHALLENGES OF THE IDEALIZED MODEL

Several comments are in order before we continue with the discussion of the more concrete experimental platforms to realize the idealized Hamiltonian in Eq. (1). First, this model has the advantage of being built upon rather common elements: the Einstein phonon is the zero-dispersion limit of an optical phonon, which is often a good approximation. More generally, optical phonons with small dispersions also work, since a mild dispersion will only contribute to the higher-order terms. Equally, the nematics DoFs are common microscopic objects, ranging in their origin from molecular anisotropy in classical liquid crystals to orbital electron DoFs in transition-metal compounds [cf. Figs. 1(a)–1(c) and Sec. VI]. The tendency towards the nematic distortion can also be emergent, for instance due to the Pomeranchuk instability of a Fermi surface [64], discussed in more detail in Sec. VI. The phonon-nematic coupling in the second term of Eq. (1) is the lowest-order coupling that respects the rotational symmetry of the system and is also generally expected, as seen in many other studies [52–56]. Hence, we expect it to be the dominant term in relevant experiments.

We note that in previous theoretical studies, the phonon-nematic coupling $\mathcal{H}_{\text{ph-nem}}$ was written for acoustic, rather than optical, phonons, as discussed in detail in Refs. [54–56]. There, although the coupling also yields a fourfold anisotropic susceptibility similar to those shown in Fig. 2, the resulting effective theory is *not* of the form of the sought-after rank-2 $U(1)$ electromagnetism. The reason for demanding a finite (albeit possibly small) energy ω_0 of optical phonons is to ensure that integrating out these higher-energy DoFs is legitimate, leading to a finite $\Lambda \equiv \lambda^2/(2m_{\text{ph}}\omega_0^2)$ in Eq. (4).

Generally, in a system with nematic and lattice degrees of freedom, one naturally expects the coupling to the *acoustic* phonons to be present. Such coupling would lead to consequences described in the previous paragraph, undesirable for the purpose of rank-2 U(1) nematic liquid. It is then necessary to design the system to avoid the target nematic degrees of freedom's coupling with the acoustic phonons. In the following section, we discuss concrete experimental setups that resolve this issue and engineer the desired coupling between the nematics and optical phonons. Briefly speaking, our construction introduces additional layers/sublattice sites with the protection of global mirror/inversion symmetry, so one symmetry sector had the gapped phonons coupled to the nematics as desired.

IV. EXPERIMENTAL PROPOSALS

To address the practical problems mentioned in the previous section, here we discuss more concrete experimental proposals in a bottom-up fashion: we start with systems described by the conventional Hamiltonian instead of the ideal one, and show how the ideal Hamiltonian can emerge by modifying these systems properly. In particular, the acoustic phonon decouples from the part described by the ideal Hamiltonian.

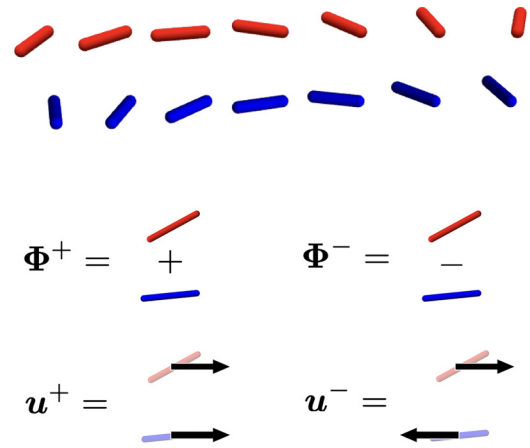

FIG. 4. A bilayer construction of two lattices with nematic degrees of freedom. The atomic lattices are not shown for clarity, but are essential in hosting intralayer acoustic phonons. The interlayer coupling results in the phonon splitting into two sectors: the acoustic in-phase mode (u^+) and the optical out-of-phase mode (u^-) in Eq. (16). These two phonon modes couple to the corresponding nematic DoFs (Ψ^+ and Ψ^-) in the appropriate sectors. It is the coupling in the out-of-phase optical sector in Eq. (17) that leads to the rank-2 U(1) theory.

A. Bilayer construction

For two-dimensional systems, one solution we propose is to construct systems with multiple sublattice sites. Here we consider an example of coupling two layers together, with each hosting the common acoustic phonon-nematic coupling [Fig. 1(d)].

Each single layer, in the most symmetric case, is described by the Hamiltonian

$$\mathcal{H}_{\text{ac-ph-nem}} = 2\rho v^2\left(\partial_i u_j^X\right)\left(\partial_i u_j^X\right) - \lambda\varepsilon_{ij}^X\Phi_{ij}^X + M\sum_{i\leqslant j}\left(\Phi_{ij}^X\right)^2. \tag{14}$$

Here, $X = \text{T}, \text{B}$ corresponds to the top and bottom layer, and the acoustic phonon modes have isotropic linear dispersion $\omega_{ac} = vq$ (again, here the dynamical terms are omitted).

We then consider the two layers coupled by the following interaction:

$$\mathcal{H}_{\text{int}} = g\rho(\mathbf{u}^{\text{T}} - \mathbf{u}^{\text{B}})^2. \tag{15}$$

Such interaction appears naturally from an interlayers' atomic potential for the lattice sites penalizing their deviation from the equilibrium positions.

Diagonalizing $\mathcal{H}_{\text{ac-ph-nem}} + \mathcal{H}_{\text{int}}$, we find that the DoF can be decomposed into the in-phase and out-of-phase sectors labeled by $+, -$ (cf. Fig. 4),

$$\begin{aligned}\boldsymbol{u}^{\pm} &= \frac{1}{\sqrt{2}}(\boldsymbol{u}^{\text{T}} \pm \boldsymbol{u}^{\text{B}}),\\ \boldsymbol{\Phi}^{\pm} &= \frac{1}{\sqrt{2}}(\boldsymbol{\Phi}^{\text{T}} \pm \boldsymbol{\Phi}^{\text{B}}).\end{aligned} \tag{16}$$

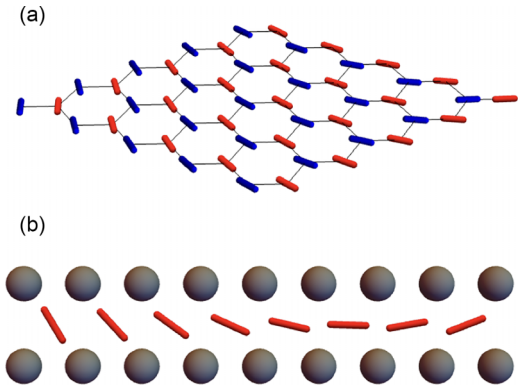

FIG. 5. Proposed experimental setups to realize the ideal model of Eq. (1). (a) The multiple sublattice site construction. Shown as an example is a hexagon lattice of nematic degrees of freedom residing on two sublattice sites (blue and red rods). (b) The artificial potential well construction. The nematic layer (red rods) is sandwiched between two substrates of heavy molecules (gray balls). The substrates serve as sources of the artificial potential term [Eq. (18)] for the lattice distortion $\boldsymbol{u}$ in the nematic layer.

The two sectors decouple from each other. The "+" sector is described again by the usual acoustic phonon-nematic coupling as in Eq. (14), and hence is not of our interest. The out-of-phase "−" sector describes the interlayer optical phonon, coupled to the corresponding interlayer nematic DoF,

$$\mathcal{H}_- = 2\rho v^2 \sum_i (\nabla u_i^-)^2 + 2g\rho \boldsymbol{u}^- \cdot \boldsymbol{u}^- - \lambda \varepsilon_{ij}^- \Phi_{ij}^- + M \sum_{i\leqslant j} \Phi_{ij}^{-2}. \tag{17}$$

Here, the phonons associated with $\boldsymbol{u}^-$ become gapped because of the interlayer coupling [Eq. (15)]. The last three terms in Eq. (17) are exactly what we are after. The first term induces the dispersion to the interlayer optical phonon. Integrating out the photons, this term yields an additional, $\mathbf{q}$-dependent contribution of the order of $O[\frac{\lambda^2 v^2 q^4}{\rho g^2}(\boldsymbol{\Phi})^2]$. This is to be compared to the principal term in the Gauss's law, of the order of $O[\frac{\lambda^2 q^2}{\rho g}(\boldsymbol{\Phi})^2]$. Hence, if the dispersion scale is small compared to the gap, i.e., $vq_0^2 \ll g$ (with $q_0 \sim 1/a$ denoting the edge of the Brillouin zone), then the phonon bands will be sufficiently flat and we obtain the idealized model of Eq. (1) to a good approximation, with $\Lambda = \frac{\lambda^2}{\rho g}$.

B. Multiple sublattice sites

The essence of the proposal in the previous section is that when there are multiple sublattice sites in the system, the total number of phonons increases accordingly, yet only one set of them is acoustic and the remaining phonon branches will become gapped, as desired to obtain the idealized model in Eq. (1). Similar approaches can be designed following this principle. For example, a single-layer nematic lattice with two sublattice sites per unit cell can also work [Fig. 5(a)].

C. Artificial potential well

Another scheme we propose is to introduce an artificial potential for the nematic-site lattice displacements, in order to break translational invariance and gap the phonons directly. That is, we add a potential term

$$\mathcal{H}_{\text{pot}} = \frac{m_{\text{ph}}\omega_0^2}{2} \boldsymbol{u} \cdot \boldsymbol{u} \tag{18}$$

to the lattice distortion, thus approximating the idealized model in Eq. (1) when the phonon dispersion is mild.

The first realization of this idea is schematically illustrated in Fig. 1(e), wherein the nematic atoms/molecules are placed in a periodic optical (laser) potential. Such periodic potential is a sophisticated experimental technique that is already in use [65–72].

Another possible realization is to sandwich the nematic layer between the substrate layers of heavy molecules. The latter would then introduce a potential term to the nematics layer, as illustrated in Fig. 5(b).

V. BEYOND THE CLASSICAL MODEL

In this work, we focused on how to achieve the electrostatics sector of the rank-2 U(1) theory. This is a crucial step toward the generalized quantum electrodynamics, just as how the classical spin ice [63] provides the underpinnings for the development of a quantum spin ice [6,12]. Now let us briefly explain the effect of including phonon and nematic dynamics in the system.

A. Phonon dynamics

Let us first examine the effect of phonon dynamics. Following the procedure similar to that outlined above Eq. (4), one can integrate the phonon kinetic term $\frac{m_{\text{ph}}}{2}(\partial_t \boldsymbol{u})^2$. This leads to the appearance in the Lagrangian of the dynamics for the nematic degrees of freedom of the form

$$\mathcal{L}_{\text{charge-dyn}} = \frac{m}{2}(\dot{\boldsymbol{\Phi}})^2 + \tilde{\Lambda}(\partial_i \dot{\Phi}_{ij})(\partial_k \dot{\Phi}_{kj}) \equiv \frac{m}{2}(\dot{\boldsymbol{\Phi}})^2 + \tilde{\Lambda}(\partial_t \boldsymbol{\rho})^2, \tag{19}$$

where $\tilde{\Lambda} = \lambda^2/(2m_{\text{ph}})$ arises from integrating out the optical phonons [in fact, $\tilde{\Lambda} = \omega_0^2 \Lambda$ is proportional to the coupling Λ introduced in Eq. (4)].

Note that the first term originates from the kinetic energy of the nematic degrees of freedom in Eq. (3). More importantly, the second term is responsible for the dynamics of the charge of the rank-2 U(1) field theory. Below, we shall consider the effect such terms have on the generalized higher-rank U(1) electrodynamics.

B. Nematic dynamics

We now discuss the effect of the dynamical term in the full-fledged rank-2 electrodynamics. We start with a concrete example and then discuss the general principles applicable to all the implementations proposed above.

For concreteness, let us consider $\boldsymbol{\Phi}$ living on the square lattice. For better visualization, we place the Φ_{xx}, Φ_{yy} components on the vertices and shift $\Phi_{xy} = \Phi_{yx}$ to the centers

of the plaquettes. This is illustrated in Figs. 3(a) and 3(b). The generalized vector charges $\boldsymbol{\rho} = (\rho_x, \rho_y)$ are then defined on the links of the lattice. Specifically, ρ_x is defined on the x-oriented links as $\rho_x = \Delta_x \Phi_{xx} + \Delta_y \Phi_{yx}$, where Δ_i is the lattice derivative. Similarly, ρ_y is defined on y links as $\rho_y = \Delta_y \Phi_{yy} + \Delta_x \Phi_{xy}$. The classical sector of the Hamiltonian is

$$\mathcal{H}_{\text{sq-cl}} = U\boldsymbol{\rho}^2 + M\sum_{i\leqslant j}\Phi_{ij}^2. \tag{20}$$

Note that we have dropped the first kinetic term $\propto (\dot{\boldsymbol{\Phi}})^2$ in Eq. (19) because, in the language of the generalized electrodynamics, $\dot{\boldsymbol{\Phi}}$ plays the role of the vector potential $\boldsymbol{A}$, canonically conjugate to the electric field $\boldsymbol{E} \equiv \boldsymbol{\Phi}$. The nematic kinetic term in Eq. (19) therefore translated into the $\boldsymbol{A}^2$ term whose action on the ground-state manifold is trivial, and hence we ignore it in what follows.

To introduce quantum dynamics, we instead argue by the way of analogy that each component of the tensor $\boldsymbol{\Phi}$ could be thought of as corresponding to the S^z component of a quantum spin, and there is a generalized "transverse field" applied to the nematic DoFs,

$$\mathcal{H}_{\text{sq-dy}} = h\sum_{i\leqslant j}(\Phi_{ij}^{+} + \Phi_{ij}^{-}), \tag{21}$$

where $\Phi_{ij}^{\pm}$ are the raising and lowering operators of Φ_{ij}. Crudely speaking, $\Phi_{ij}^{\pm}$ plays the role of the gauge field operator $\boldsymbol{A}$ associated with the charge creation terms since they are canonically conjugate to the electric field components $\boldsymbol{E}$, and creates charges when applied to an eigenstate of Φ_{ij}.

A single operation of $\Phi_{xx}^{\pm}$ or $\Phi_{yy}^{\pm}$ will create charges in the system. Within the restricted sub-Hilbert space of the Gauss's law-obeying states, operators $\Phi_{ij}^{\pm}$ can only act on the Hilbert space at a higher perturbative order, such as to cancel all the charges that are created. An example, which we denote as Φ_{comp}^{+}, is shown in Fig. 3(e). There, a specific product of 12 $\Phi_{ij}^{\pm}$ operators connects one charge-free electric field configuration to another. The fact that no charge is created anywhere in the system is equivalent to the statement that this composite product of 12 operators is gauge invariant—that is, Φ_{comp}^{+} (and also its Hermitian conjugate Φ_{comp}^{-}) plays the role of the generalized magnetic field of the R2-U1 theory.

Putting everything together, the generalized rank-2 electrodynamics is realized by the Hamiltonian

$$\begin{aligned}\mathcal{H}_{\text{sq-full}} &= \tilde{\Lambda}(\partial_t \boldsymbol{\rho})^2 + U\boldsymbol{\rho}^2 + M\sum_{i\leqslant j}\Phi_{ij}^2 + \mu(\Phi_{\text{comp}}^{-} + \Phi_{\text{comp}}^{+}) \\ &\sim \tilde{\Lambda}(\partial_t \boldsymbol{\rho})^2 + U\boldsymbol{\rho}^2 + \boldsymbol{E}^2 + \boldsymbol{B}^2.\end{aligned} \tag{22}$$

Now let us comment on the general properties of the quantum dynamics of the nematic R2-U1 theory. Like in a quantum spin ice, the emergent magnetic field usually involves multiple operators, and is perturbatively generated via the product of transverse field operators which preserve the Gauss's law. Other types of dynamics, for example, the exchange-type terms, can also fulfill this purpose. In the conventional Maxwell U(1) theory, these composite operators are simply loops of the dynamical operators, forming a lattice realization of the magnetic flux $\oint \boldsymbol{A}\,\mathrm{d}\boldsymbol{l} = \iint \boldsymbol{B}\,\mathrm{d}\sigma$. In R2-U1 theory, the composite operators become more complicated, as shown in the square lattice example above.

Although the long-wavelength theory will remain the same, the available quantum dynamical terms will depend on the details of the lattice geometry and the microscopic implementation of the nematic DoF. It is also possible that the quantum dynamics leads the system into other ordered phases instead of R2-U1 electrodynamics (this is true of the quantum spin ice as well). The exact consequences will have to be discussed on a case-by-case basis.

VI. DISCUSSION: MICROSCOPIC ORIGIN OF THE NEMATICS

In our construction, we tacitly assumed that the nematic DoFs are described by a symmetric tensor with all its independent components, of which there are three in the two-dimensional systems and five in the three-dimensional ones. Depending on the microscopic origin of the nematics, the number of DoFs in the symmetric tensor representation may be fewer than those numbers. Below, we provide several concrete examples of the various microscopic realizations of the nematic DoFs.

Liquid crystals. The first canonical example of the nematic degrees of freedom is that of a classical liquid crystal. In two dimensions (2D), such as schematically shown in Fig. 1(b), the nematicity is described by a director of a fixed length, encoded in a 2×2 symmetric matrix,

$$\boldsymbol{\Phi} = \begin{pmatrix} \cos 2\theta & \sin 2\theta \\ \sin 2\theta & -\cos 2\theta \end{pmatrix}. \tag{23}$$

Note that the matrix is traceless and unimodular (reflecting the fact that the director is of unit length) and, as a result, nematic DoFs are described not by three, but by a single independent parameter, i.e., the azimuthal angle θ. The idealized theory presented in the beginning still holds; however, the lack of the necessary rank-2 DoFs means the proper R2-U1 electrostatics cannot be realized.

Pomeranchuk instability in metals. Another example of the nematicity is the spontaneous distortion of the Fermi surface [see, e.g., Fig. 1(c)], known as the Pomeranchuk instability [64], which, in the simplest case of an isotropic (circular in 2D) Fermi surface, is described by the quadrupole density operator [73],

$$\boldsymbol{\Phi}_{FS}(\boldsymbol{q}) = \frac{1}{k_F^2}\psi^{\dagger}(\boldsymbol{q})\begin{pmatrix} q_x^2 - q_y^2 & q_x q_y \\ q_x q_y & q_y^2 - q_x^2 \end{pmatrix}\psi(\boldsymbol{q}), \tag{24}$$

where $\psi^{\dagger}(\boldsymbol{q})$ and $\psi(\boldsymbol{q})$ are the electron creation/annihilation operators at momentum $\boldsymbol{q}$. The above matrix is also traceless, yielding the traceless R2-U1 theory upon integration of the phonon modes coupled to $\boldsymbol{\Phi}_{FS}$ as in Eq. (1). The elliptic Fermi surface distortion thus has two independent DoFs: Φ_{xx} and Φ_{xy}, which can also be cast in the form of a complex order parameter $Qe^{i2\theta} = \Phi_{xx} + i\Phi_{xy}$, with the amplitude Q proportional to the eccentricity of the ellipse and angle $\pm\theta$ its azimuthal direction.

We note that in the above example, the presence of the underlying crystalline lattice can pin the Fermi surface distortion along particular direction(s), such as shown in Fig. 1(c).

For instance, pinning to $\pm x$ or $\pm y$ directions on the square lattice introduces a potential $U_{\text{lat}}(\theta) = -U_0 \cos(2\theta)$ for the azimuthal angle. The resulting rank-2 theory would then become discrete, described by a four-state Potts model on a square lattice [rather than the continuous U(1) parameter]. Nevertheless, for temperatures and energy scales above U_0, the classical theory could be approximately described as having a continuous U(1) symmetry.

A remark is due: In this and in other examples of metallic systems with nematic degrees of freedom, coupling of the latter to the conduction electrons must be considered carefully, especially in two spatial dimensions. In particular, at the nematic quantum critical point, when the parameter $M \to 0$ in the Hamiltonian (1), this coupling renormalizes the Green's function of the conduction electrons, resulting in a non-Fermi-liquid behavior and in turn affecting the universality class of the nematic phase transition [74] (see, also, Ref. [75] for review, as well as recent numerical studies [76,77] and references therein). These considerations lie outside of the scope of the present work, and we will always assume a large and positive quadratic coefficient M where these complications do not arise.

Orbital order in Mott insulators. Another example is that of d-electron orbital ordering in Mott insulators such as K_2CuF_4 [78] and $LaMnO_3$ [79] [Fig. 1(a)]. Ignoring, for the moment, the crystal electric field (CEF) effects, which generically lift the orbital SO(3) symmetry, the five d orbitals corresponding to the $|l = 2; m = -2, -1, \ldots, 2\rangle$ spherical harmonics form a degenerate manifold, out of which an orbital-nematic order can appear if the symmetry is spontaneously broken. These orbital degrees of freedom form a symmetric, traceless tensor representation of the group SO(3) describing rotations in the orbital Hilbert space (the $l = 0, 1$ representations are the trace and antisymmetric components of this matrix). In the disordered, symmetry-preserving phase, these orbital degrees of freedom can be used to construct *classical* rank-2 electrostatics, as outlined in this work. Moreover, by virtue of being intrinsically quantum objects, such models are also good candidates for constructing *quantum* electrodynamics of R2-U1 theory. This line of argument can be expanded to higher multipole ordering, such as octupolar (rank-3) order observed in $Ce_xLa_{1-x}B_6$ [80] and hexadecupolar (rank-4) [81] and even higher rank-5 order parameters [82] proposed to explain the so-called hidden order in URu_2Si_2 [83].

When the CEF effects are considered, the initial degeneracy of the d-orbital multiplet is lifted; however, as long as the symmetry is not too low and the crystalline point group allows for higher-dimensional irreducible representations (irreps), the description in terms of the higher-rank tensor survives, as we shall now discuss.

Multidimensional irreps of the crystalline symmetry. This is a generic example of (discrete) nematic order that is realized on crystalline lattices with n-fold irreducible representations ($n = 2, 3$) of the point group. For instance, hexagonal systems (with point groups C_6 and D_6 in 2D) allow two-dimensional irreducible representations and hence the nematic order parameter can be parametrized by $\mathbf{\Phi} = \Phi_0[\cos(2\theta), \sin(2\theta)]$, which can be cast in the form of a traceless rank-2 tensor as in Eq. (23). This well-known fact has been exploited recently in the discussion of nematicity in twisted bilayer graphene, where coupling to acoustic phonons (different from the optical phonons in our case) was also considered [56]. Generically, the lattice pinning will result in a discrete Potts model description of the nematic DoF, analogous to the previous case, and upon integrating out the (optical) phonons, the resulting rank-2 theory will be a discrete one.

When designing possible experimental realizations of the nematic-phonon coupling, one should thus be aware of the consequence of such discretization and the decreased number of DoFs (as exemplified by the traceless condition in the second and third examples above), since too few DoFs may result in ordered phases or states with subsystem symmetries only. This, however, could also be a blessing in disguise since it means we have a wider range of R2–U1 theories accessible in an experiment. A particularly interesting type of such theories, for instance, is built in 3D from tensors with all diagonal components vanishing. Such "hollow" rank-2 theories turn out to be the gateways toward gapped fracton order upon "Higgsing" the rank-2 U(1) degrees of freedom [34,35]. The resulting gapped fracton orders hold great potential for applications in quantum memory storage.

In summary, we presented a theoretical model with simple ingredients that can realize the emergent rank-2 U(1) electrostatics via optical phonon-nematic coupling. Given the intimate connection between this rank-2 generalized electrodynamics and the exotic fracton phases of matter [26,28] which have recently garnered much attention, the present work thus paves the way towards natural implementations of the fracton matter in the experiment. Given the simplicity of the ingredients (optical phonons and nematic DoF), we hope this proposal may be realized in various settings, from liquid crystals to bilayer systems to polar molecules in a periodic optical potential, and we have outlined several such possible constructions. The present proposal yields a classical rank-2 theory, which is a necessary first step on the path towards truly quantum rank-2 electrodynamics and fracton physics. We have outlined a possible route towards such quantum theory by incorporating the dynamics of the generalized magnetic fields into our nematic model.

ACKNOWLEDGMENTS

The authors thank Leo Radzihovsky for discussions. This work was supported by the National Science Foundation, Division of Materials Research, under the Award No. DMR-1917511.

APPENDIX A: BRIEF REVIEW OF RANK-2 U(1) GAUGE THEORY

We start by briefly reviewing a version of rank-2 U(1) gauge theory, which is to be realized in the models we propose in this paper.

As its name suggests, the R2-U1 gauge theory uses rank-2 tensors E_{ij} and A_{ij} as its electric and gauge field instead of vectors. More specifically, the tensor field is symmetric,

$$E_{ij} = E_{ji} \quad A_{ij} = A_{ji}. \tag{A1}$$

The charge is a vector defined as

$$\rho_i = \partial^k \mathrm{E}_{ki}\,. \tag{A2}$$

The low-energy sector of the theory has to be charge free,

$$\partial^k E_{ki} = 0, \tag{A3}$$

which dictates the form of the gauge-invariance condition,

$$A_{ij} \to A_{ij} + \partial_i \lambda_j + \partial_i \lambda_j. \tag{A4}$$

The magnetic field is the simplest object that is gauge invariant,

$$B_{ij} = \epsilon_{iab}\epsilon_{jcd}\partial^a \partial^c A^{bd}. \tag{A5}$$

One can now write down the Hamiltonian for the R2-U1 gauge theory as

$$\begin{aligned}\mathcal{H}_{\text{R2-U1}} &= U\,\partial^k E_{ki}\partial^l E_{li} + E_{ij}E_{ij} + B_{ij}B_{ij} \\ &= U\,\boldsymbol{\rho}^2 + \boldsymbol{E}^2 + \boldsymbol{B}^2.\end{aligned} \tag{A6}$$

Here we assumed the Einstein's summation rule, while not caring about the super- and subscripts.

Our aim in this paper is to find out a general, and experimentally realistic, route to realize the classical part of this Hamiltonian

$$\mathcal{H}_{\text{R2-U1-cl}} = U\,\boldsymbol{\rho}^2 + \boldsymbol{E}^2. \tag{A7}$$

The quantum dynamics, i.e., the $\boldsymbol{B}^2$ term, is also possible to realize, but is highly dependent on the specific setup of the physical system. It will not be a focus of this paper.

APPENDIX B: SELF-CONSISTENT GAUSSIAN APPROXIMATION

The self-consistent Gaussian approximation (SCGA) is an analytical method that treats the nematics in the large-N limit, which is known to produce rather accurate results in the spin/nematic liquid phases. Our calculation closely follows the exposition in Ref. [84]. We first treat Φ_{ij} as an independent, freely fluctuating DoF. The Hamiltonian in the momentum space is written as

$$\mathcal{E}_{\text{Large-}N} = \tfrac{1}{2}\tilde{\boldsymbol{\Phi}}\mathcal{H}_{\text{Large-}N}\tilde{\boldsymbol{\Phi}}^T, \tag{B1}$$

in terms of the triad of nematic components (for the two-dimensional model) $\tilde{\boldsymbol{\Phi}} = (\Phi_{xx}, \Phi_{yy}, \Phi_{xy})$. The matrix $H_{\text{Large}-N}$ is the Fourier transformed interaction matrix from Eq. (4),

$$H_{\text{Large-}N} = 2\Lambda \begin{pmatrix} C_x^2 & 0 & C_xC_y \\ 0 & C_y^2 & C_xC_y \\ C_xC_y & C_xC_y & C_x^2 + C_y^2 \end{pmatrix}, \tag{B2}$$

where C_x and C_y are the momentum-dependent functions. For the square lattice model (Fig. 3), $C_x = 2\sin(q_x/2)$, $C_y = 2\sin(q_y/2)$, with the lattice constant set to 1.

We then introduce a Lagrange multiplier with coefficient $\mu(\beta)$ to the partition function to obtain

$$\mathcal{Z} = \exp\left\{-\frac{1}{2}\int_{\text{BZ}} \mathrm{d}\boldsymbol{q} \int \mathrm{d}\tilde{\boldsymbol{\Phi}}\tilde{\boldsymbol{\Phi}}[\beta\mathcal{H}_{\text{Large-}N} + \mu(\beta)\mathcal{I}]\tilde{\boldsymbol{\Phi}}^T\right\}, \tag{B3}$$

where β denotes the inverse temperature. The purpose of the term $\mu(\beta)\tilde{\boldsymbol{\Phi}}\mathcal{I}\tilde{\boldsymbol{\Phi}}^T$ ($\mathcal{I}$ stands for the identity matrix) is to impose, on average, an additional unimodular constraint on the nematic DoF, such that

$$\left\langle \Phi_{xx}^2 + \Phi_{yy}^2 + \Phi_{xy}^2 \right\rangle = 1. \tag{B4}$$

For a given temperature $T = 1/\beta$, the value of $\mu(\beta)$ is numerically obtained by searching for its value that must satisfy the constraint

$$\int_{\text{BZ}} \mathrm{d}\boldsymbol{q} \sum_{i=1}^{3} \frac{1}{\lambda_i(\boldsymbol{q}) + \mu(\beta)} = \left\langle \Phi_{xx}^2 + \Phi_{yy}^2 + \Phi_{xy}^2 \right\rangle = 1, \tag{B5}$$

where $\lambda_i(\boldsymbol{q})$, $i = 1, 2, 3$ are the three eigenvalues of $\beta\mathcal{H}_{\text{Large-}N}(\boldsymbol{q})$.

With μ fixed, the partition function is completely determined for a free theory of $\tilde{\boldsymbol{\Phi}}$, and all correlation functions in Fig. 2 can be computed by extracting the corresponding components in $[\beta\mathcal{H}_{\text{Large-N}} + \mu(\beta)\mathcal{I}]^{-1}$.

[1] P. W. Anderson, More is different, Science **177**, 393 (1972).

[2] P. Anderson, Resonating valence bonds: A new kind of insulator? Mater. Res. Bull. **8**, 153 (1973).

[3] L. Balents, Spin liquids in frustrated magnets, Nature (London) **464**, 199 (2010).

[4] L. Savary and L. Balents, Quantum spin liquids: A review, Rep. Prog. Phys. **80**, 016502 (2017).

[5] Y. Zhou, K. Kanoda, and T.-K. Ng, Quantum spin liquid states, Rev. Mod. Phys. **89**, 025003 (2017).

[6] M. Hermele, M. P. A. Fisher, and L. Balents, Pyrochlore photons: The U(1) spin liquid in a $S = \frac{1}{2}$ three-dimensional frustrated magnet, Phys. Rev. B **69**, 064404 (2004).

[7] A. Banerjee, S. V. Isakov, K. Damle, and Y. B. Kim, Unusual liquid state of hard-core bosons on the pyrochlore lattice, Phys. Rev. Lett. **100**, 047208 (2008).

[8] O. Benton, O. Sikora, and N. Shannon, Seeing the light: Experimental signatures of emergent electromagnetism in a quantum spin ice, Phys. Rev. B **86**, 075154 (2012).

[9] L. Savary and L. Balents, Coulombic quantum liquids in spin-1/2 pyrochlores, Phys. Rev. Lett. **108**, 037202 (2012).

[10] N. Shannon, O. Sikora, F. Pollmann, K. Penc, and P. Fulde, Quantum ice: A quantum Monte Carlo study, Phys. Rev. Lett. **108**, 067204 (2012).

[11] Z. Hao, A. G. R. Day, and M. J. P. Gingras, Bosonic many-body theory of quantum spin ice, Phys. Rev. B **90**, 214430 (2014).

[12] M. J. P. Gingras and P. A. McClarty, Quantum spin ice: A search for gapless quantum spin liquids in pyrochlore magnets, Rep. Prog. Phys. **77**, 056501 (2014).

[13] Y. Kato and S. Onoda, Numerical evidence of quantum melting of spin ice: Quantum-to-classical crossover, Phys. Rev. Lett. **115**, 077202 (2015).

[14] G. Chen, Dirac's "magnetic monopoles" in pyrochlore ice $u(1)$ spin liquids: Spectrum and classification, Phys. Rev. B **96**, 195127 (2017).

[15] C.-J. Huang, Y. Deng, Y. Wan, and Z. Y. Meng, Dynamics of topological excitations in a model quantum spin ice, Phys. Rev. Lett. **120**, 167202 (2018).

[16] H. D. Zhou, C. R. Wiebe, J. A. Janik, L. Balicas, Y. J. Yo, Y. Qiu, J. R. D. Copley, and J. S. Gardner, Dynamic spin ice: $Pr_2Sn_2O_7$, Phys. Rev. Lett. **101**, 227204 (2008).

[17] K. A. Ross, L. Savary, B. D. Gaulin, and L. Balents, Quantum excitations in quantum spin ice, Phys. Rev. X **1**, 021002 (2011).

[18] T. Fennell, M. Kenzelmann, B. Roessli, M. K. Haas, and R. J. Cava, Power-law spin correlations in the pyrochlore antiferromagnet $Tb_2Ti_2O_7$, Phys. Rev. Lett. **109**, 017201 (2012).

[19] K. Kimura, S. Nakatsuji, J.-J. Wen, C. Broholm, M. B. Stone, E. Nishibori, and H. Sawa, Quantum fluctuations in spin-ice-like $Pr_2Zr_2O_7$, Nat. Commun. **4**, 1934 (2013).

[20] R. Sibille, E. Lhotel, V. Pomjakushin, C. Baines, T. Fennell, and M. Kenzelmann, Candidate quantum spin liquid in the Ce^{3+} pyrochlore stannate $Ce_2Sn_2O_7$, Phys. Rev. Lett. **115**, 097202 (2015).

[21] J.-J. Wen, S. M. Koohpayeh, K. A. Ross, B. A. Trump, T. M. McQueen, K. Kimura, S. Nakatsuji, Y. Qiu, D. M. Pajerowski, J. R. D. Copley, and C. L. Broholm, Disordered route to the coulomb quantum spin liquid: Random transverse fields on spin ice in $Pr_2Zr_2O_7$, Phys. Rev. Lett. **118**, 107206 (2017).

[22] J. D. Thompson, P. A. McClarty, D. Prabhakaran, I. Cabrera, T. Guidi, and R. Coldea, Quasiparticle breakdown and spin hamiltonian of the frustrated quantum pyrochlore $Yb_2Ti_2O_7$ in a magnetic field, Phys. Rev. Lett. **119**, 057203 (2017).

[23] R. Sibille, N. Gauthier, H. Yan, M. Ciomaga Hatnean, J. Ollivier, B. Winn, U. Filges, G. Balakrishnan, M. Kenzelmann, N. Shannon, and T. Fennell, Experimental signatures of emergent quantum electrodynamics in $Pr_2Hf_2O_7$, Nat. Phys. **14**, 711 (2018).

[24] B. Gao, T. Chen, D. W. Tam, C.-L. Huang, K. Sasmal, D. T. Adroja, F. Ye, H. Cao, G. Sala, M. B. Stone, C. Baines, J. A. T. Verezhak, H. Hu, J.-H. Chung, X. Xu, S.-W. Cheong, M. Nallaiyan, S. Spagna, M. B. Maple, A. H. Nevidomskyy *et al.*, Experimental signatures of a three-dimensional quantum spin liquid in effective spin-1/2 $Ce_2Zr_2O_7$ pyrochlore, Nat. Phys. **15**, 1052 (2019).

[25] C. Xu, An algebraic spin liquid with soft gravitons, Phys. Rev. B **74**, 224433 (2006).

[26] M. Pretko, Generalized electromagnetism of subdimensional particles: A spin liquid story, Phys. Rev. B **96**, 035119 (2017).

[27] A. Rasmussen, Y.-Z. You, and C. Xu, Stable gapless Bose liquid phases without any symmetry, arXiv:1601.08235.

[28] M. Pretko, Subdimensional particle structure of higher rank $u(1)$ spin liquids, Phys. Rev. B **95**, 115139 (2017).

[29] C. Chamon, Quantum glassiness in strongly correlated clean systems: An example of topological overprotection, Phys. Rev. Lett. **94**, 040402 (2005).

[30] N. Shannon, G. Misguich, and K. Penc, Cyclic exchange, isolated states, and spinon deconfinement in an *XXZ* Heisenberg model on the checkerboard lattice, Phys. Rev. B **69**, 220403(R) (2004).

[31] J. Haah, Local stabilizer codes in three dimensions without string logical operators, Phys. Rev. A **83**, 042330 (2011).

[32] S. Vijay, J. Haah, and L. Fu, A new kind of topological quantum order: A dimensional hierarchy of quasiparticles built from stationary excitations, Phys. Rev. B **92**, 235136 (2015).

[33] S. Vijay, J. Haah, and L. Fu, Fracton topological order, generalized lattice gauge theory, and duality, Phys. Rev. B **94**, 235157 (2016).

[34] D. Bulmash and M. Barkeshli, Higgs mechanism in higher-rank symmetric U(1) gauge theories, Phys. Rev. B **97**, 235112 (2018).

[35] H. Ma, M. Hermele, and X. Chen, Fracton topological order from the Higgs and partial-confinement mechanisms of rank-two gauge theory, Phys. Rev. B **98**, 035111 (2018).

[36] R. M. Nandkishore and M. Hermele, Fractons, Annu. Rev. Condens. Matter Phys. **10**, 295 (2019).

[37] K. Slagle and Y. B. Kim, Fracton topological order from nearest-neighbor two-spin interactions and dualities, Phys. Rev. B **96**, 165106 (2017).

[38] G. B. Halász, T. H. Hsieh, and L. Balents, Fracton topological phases from strongly coupled spin chains, Phys. Rev. Lett. **119**, 257202 (2017).

[39] A. T. Schmitz, H. Ma, R. M. Nandkishore, and S. A. Parameswaran, Recoverable information and emergent conservation laws in fracton stabilizer codes, Phys. Rev. B **97**, 134426 (2018).

[40] A. Kubica and B. Yoshida, Ungauging quantum errorcorrecting codes, arXiv:1805.01836.

[41] O. Benton, L. D. C. Jaubert, H. Yan, and N. Shannon, spin-liquid with pinch-line singularities on the pyrochlore lattice, Nat. Commun. **7**, 11572 (2016).

[42] M. Pretko, Emergent gravity of fractons: Mach's principle revisited, Phys. Rev. D **96**, 024051 (2017).

[43] H. Yan, Hyperbolic fracton model, subsystem symmetry, and holography, Phys. Rev. B **99**, 155126 (2019).

[44] M. Pretko and L. Radzihovsky, Fracton-elasticity duality, Phys. Rev. Lett. **120**, 195301 (2018).

[45] A. Gromov, Chiral topological elasticity and fracton order, Phys. Rev. Lett. **122**, 076403 (2019).

[46] Y. You, J. Bibo, F. Pollmann, and T. L. Hughes, Fracton critical point in higher-order topological phase transition, arXiv:2008.01746.

[47] Z. Zhou, X.-F. Zhang, F. Pollmann, and Y. You, Fractal quantum phase transitions: Critical phenomena beyond renormalization, arXiv:2105.05851.

[48] Y. You, F. J. Burnell, and T. L. Hughes, Multipolar topological field theories: Bridging higher order topological insulators and fractons, Phys. Rev. B **103**, 245128 (2021).

[49] C. Xu and P. Hořava, Emergent gravity at a lifshitz point from a bose liquid on the lattice, Phys. Rev. D **81**, 104033 (2010).

[50] C. Xu and M. P. A. Fisher, Bond algebraic liquid phase in strongly correlated multiflavor cold atom systems, Phys. Rev. B **75**, 104428 (2007).

[51] Y. You and F. von Oppen, Building fracton phases by majorana manipulation, Phys. Rev. Res. **1**, 013011 (2019).

[52] R. A. Cowley, Acoustic phonon instabilities and structural phase transitions, Phys. Rev. B **13**, 4877 (1976).

[53] U. Karahasanovic and J. Schmalian, Elastic coupling and spin-driven nematicity in iron-based superconductors, Phys. Rev. B **93**, 064520 (2016).

[54] I. Paul and M. Garst, Lattice effects on nematic quantum criticality in metals, Phys. Rev. Lett. **118**, 227601 (2017).

[55] V. S. de Carvalho and R. M. Fernandes, Resistivity near a nematic quantum critical point: Impact of acoustic phonons, Phys. Rev. B **100**, 115103 (2019).

[56] R. M. Fernandes and J. W. F. Venderbos, Nematicity with a twist: Rotational symmetry breaking in a moiré superlattice, Sci. Adv. **6**, eaba8834 (2020).
[57] Otherwise (if mass $M < 0$), one would need to include quartic terms of the type $[\mathrm{Tr}(\Phi^2)]^2$ to stabilize the theory.
[58] J. Nehring and A. Saupe, On the schlieren texture in nematic and smectic liquid crystals, J. Chem. Soc. Faraday Trans. **68**, 1 (1972).
[59] C. Chiccoli, I. Feruli, O. D. Lavrentovich, P. Pasini, S. V. Shiyanovskii, and C. Zannoni, Topological defects in schlieren textures of biaxial and uniaxial nematics, Phys. Rev. E **66**, 030701(R) (2002).
[60] A. Prem, S. Vijay, Y.-Z. Chou, M. Pretko, and R. M. Nandkishore, Pinch point singularities of tensor spin liquids, Phys. Rev. B **98**, 165140 (2018).
[61] H. Yan, O. Benton, L. D. C. Jaubert, and N. Shannon, Rank-2 $u(1)$ spin liquid on the breathing pyrochlore lattice, Phys. Rev. Lett. **124**, 127203 (2020).
[62] O. Benton and R. Moessner, Topological route to new and unusual coulomb spin liquids, Phys. Rev. Lett. **127**, 107202 (2021).
[63] S. T. Bramwell and M. J. P. Gingras, Spin ice state in frustrated magnetic pyrochlore materials, Science **294**, 1495 (2001).
[64] I. I. Pomeranchuk, On the stability of a fermi liquid, Zh. Eksp. Teor. Fiz. **35**, 524 (1958).
[65] R. Grimm, M. Weidemüller, and Y. B. Ovchinnikov, Optical dipole traps for neutral atoms, in *Advances In Atomic, Molecular, and Optical Physics*, edited by B. Bederson and H. Walther (Elsevier, Amsterdam, The Netherlands, 2000), pp. 95–170.
[66] I. Bloch, Ultracold quantum gases in optical lattices, Nat. Phys. **1**, 23 (2005).
[67] M. Greiner, O. Mandel, T. Esslinger, T. W. Hänsch, and I. Bloch, Quantum phase transition from a superfluid to a Mott insulator in a gas of ultracold atoms, Nature (London) **415**, 39 (2002).
[68] W. S. Bakr, J. I. Gillen, A. Peng, S. Fölling, and M. Greiner, A quantum gas microscope for detecting single atoms in a Hubbard-regime optical lattice,Nature (London) **462**, 74 (2009).
[69] B. Yang, H. Sun, C.-J. Huang, H.-Y. Wang, Y. Deng, H.-N. Dai, Z.-S. Yuan, and J.-W. Pan, Cooling and entangling ultracold atoms in optical lattices, Science **369**, 550 (2020).
[70] M. P. MacDonald, G. C. Spalding, and K. Dholakia, Microfluidic sorting in an optical lattice, Nature (London) **426**, 421 (2003).
[71] I. Bloch, J. Dalibard, and W. Zwerger, Many-body physics with ultracold gases, Rev. Mod. Phys. **80**, 885 (2008).
[72] A. Eckardt, Colloquium: Atomic quantum gases in periodically driven optical lattices, Rev. Mod. Phys. **89**, 011004 (2017).
[73] V. Oganesyan, S. A. Kivelson, and E. Fradkin, Quantum theory of a nematic fermi fluid, Phys. Rev. B **64**, 195109 (2001).
[74] M. A. Metlitski and S. Sachdev, Quantum phase transitions of metals in two spatial dimensions. I. Ising-nematic order, Phys. Rev. B **82**, 075127 (2010).
[75] E. Fradkin, S. A. Kivelson, M. J. Lawler, J. P. Eisenstein, and A. P. Mackenzie, Nematic fermi fluids in condensed matter physics, Annu. Rev. Condens. Matter Phys. **1**, 153 (2010).
[76] Y. Schattner, S. Lederer, S. A. Kivelson, and E. Berg, Ising nematic quantum critical point in a metal: A Monte Carlo study, Phys. Rev. X **6**, 031028 (2016).
[77] X. Y. Xu, Z. H. Liu, G. Pan, Y. Qi, K. Sun, and Z. Y. Meng, Revealing fermionic quantum criticality from new Monte Carlo techniques, J. Phys.: Condens. Matter **31**, 463001 (2019).
[78] D. I. Khomskii and K. I. Kugel, Orbital and magnetic structure of two-dimensional ferromagnets with Jahn-Teller ions, Solid State Commun. **13**, 763 (1973).
[79] R. Shiina, T. Nishitani, and H. Shiba, Magnetic ordering, orbital state and lattice distortion in perovskite manganites, J. Phys. Soc. Jpn. **66**, 3159 (1997).
[80] D. Mannix, Y. Tanaka, D. Carbone, N. Bernhoeft, and S. Kunii, Order parameter segregation in $Ce_{0.7}La_{0.3}B_6$: 4f octopole and 5d dipole magnetic order, Phys. Rev. Lett. **95**, 117206 (2005).
[81] K. Haule and G. Kotliar, Arrested Kondo effect and hidden order in URu_2Si_2, Nat. Phys. **5**, 796 (2009).
[82] H. Ikeda, M.-T. Suzuki, R. Arita, T. Takimoto, T. Shibauchi, and Y. Matsuda, Emergent rank-5 nematic order in URu_2Si_2, Nat. Phys. **8**, 528 (2012).
[83] J. A. Mydosh, P. M. Oppeneer, and P. S. Riseborough, Hidden order and beyond: an experimentaltheoretical overview of the multifaceted behavior of URu_2Si_2, J. Phys.: Condens. Matter **32**, 143002 (2020).
[84] S. V. Isakov, K. Gregor, R. Moessner, and S. L. Sondhi, Dipolar spin correlations in classical pyrochlore magnets, Phys. Rev. Lett. **93**, 167204 (2004).